TITLE OF PROJECT:

FE0002225: Actualistic and geochemical modeling of reservoir rock, CO_2 and formation fluid interaction, Citronelle oil field, Alabama

Final Technical Report for
DE-FOA-0000032 GEOLOGIC SEQUESTRATION TRAINING AND RESEARCH

SUBMITTED BY:
West Virginia University
PO Box 6216
Morgantown, WV
Phone: (304) 293-3449
Fax: (304) 293-7498

DATE:
10/14/14

PRINCIPAL INVESTIGATOR:
Amy Weislogel
West Virginia University
(304) 293-6721
Fax: (304) 293-6522
amy.weislogel@mail.wvu.edu

CO-PRINCIPAL INVESTIGATOR:
Rona Donahoe
University of Alabama
(205) 348-1879
Fax: (205) 348-0818
rdonahoe@geo.ua.edu

SUBMITTED TO:
U. S. Department of Energy
National Energy Technology Laboratory

DISCLAIMER

ABSTRACT

This report includes description of the Citronelle field study area and the work carried out in the project to characterize the geology and composition of reservoir rock material and to collect an analyze the geochemical composition of produced fluid waters from the Citronelle field. Reservoir rock samples collected from well bore core were made into thin-sections and assessed for textural properties, including pore types and porosity distribution. Compositional framework grain modal data were collected via point-counting, and grain and cement mineralogy was assessed using SEM-EDS. Geochemistry of fluid samples is described and modeled using PHREEQC. Composition of rock and produced fluids were used as inputs for TOUGHREACT reactive transport modeling, which determined the rock-fluid system was in disequilibrium.

TABLE OF CONTENTS

EXECUTIVE SUMMARY

To better constrain short- and long-term changes in formation matrix geochemistry and permeability that affects the long-term storage capacity and EOR production of the reservoir, this study aimed at developing a model of fluid-rock interaction through study of reservoir rock samples from conventional core and formation fluid samples obtained at the well head. Results from work on this project include sampling cores from 7 wells, including the CO_2 injector well (Permit 3232) in order to determine the diagenetic history of the Donovan Sand reservoir. Thin-sectioned reservoir rock samples were analyzed using petrographic optical microscopy, combined SEM imaging and EDS analyses, and RAMAN spectroscopy. Point counting framework grain composition, porosity photometric analysis, and intergranular phase identification were conducted to develop a paragenetic model, which indicates that carbonate cementation and feldspar dissolution variably occurred during burial and subsequent diagenesis, and served as the main control on primary and secondary porosity development. We hypothesize that carbonic and sulfuric acid associated with hydrocarbon charging aided in dissolution of feldspar and clay weathering products. The removal of hydrocarbons from grain surfaces during EOR may lead to continued secondary porosity development via acidic or acidified formation waters, thus in essence making the diageneitc history of Donovan sandstone a predictive analog for future rock-fluid interactions. We predict that the heterogeneity of the Donovan Sand developed from polyphase mineral precipitation and dissolution in the reservoir matrix is likely responsible for forming preferential flow paths within high porosity zones of the reservoir. Viscous fingering of CO_2 due to differential flow along theses paths could have resulted in the initial increase and subsequent decline in CO_2-EOR of the Donovan Sandstone.

Analyses of aqueous fluid geochemistry was accomplished through pH measurement, inductively coupled plasma optical emission spectroscopy (ICP-OES), ion chromatography (IC), and inductively coupled plasma mass spectroscopy (ICP-MS) analyses of formation fluid waters and Citronelle City water. PHREEQC modeling of aqueous fluid geochemical data was attempted by first developing a VBA macro for data input into PHREEQC. Initial temporal modeling results for pH, Fe and mineral saturation indices were generated and show changes from the transition from CO2 injection and then through the duration of the subsequent water flood. A working physical model of rock-fluid interactions could not be obtained for this system, likely due to, rock and fluid heterogeneity, fracture-dominated flow system. The 2-D and 1-D TOUGHREACT models produced to date have failed to give realistic breakthrough times for both CO2 and waterflood fluids, and do not result in reasonable predictions for

either the chemistry or temporal composition trends for the produced water samples collected in this study. Initial problems with injection of CO2 almost certainly resulted in NE-SW vertical fracturing of the reservoir. This hypothesis is supported by both water chemistry and oil production data. The presence of the fracturing is a major control on the chemical composition of the produced water samples and has presented serious challenges for constructing a reactive transport model for the system. Results from this project were presented by project PI and co-PI as well as student research assistants at approximately 12 conferences. Abstracts and technical reports generated the project are archived on the project website.

NTRODUCTION

Geological sequestration of carbon dioxide for enhanced oil recovery (EOR) represents a long-term, practical means of mitigating the effects of greenhouse gas emissions to the atmosphere on global climate, while simultaneously extending the production life of a mature oil field. This project aimed to model fluid-rock interaction of the Donovan sandstone of the Rodessa Formation, an oil-bearing reservoir unit in the Citronelle Field of southwest Alabama in order to predict any reactivity of the reservoir rock in response to CO_2 injection and subsequent water flooding

The Citronelle Field is located at the apex of the broad, salt-cored Citronelle Dome that lies along the border of Mobile and Washington counties, Alabama, USA (**Figure 1**). The field produces primarily oil from the Donovan Sandstone of the middle Cretaceous (Albian) Rodessa Formation, with the underlying Jurassic Smackover Formation as the inferred hydrocarbons source (Claypool and Mancini, 1989; Pashin et al., 2007; Mancini and Puckett, 2002). The Rodessa Formation consists of arkosic sandstone, siltstone and shale with interbedded intrabasinal conglomeratic sandstones, and is approximately 244 m (800 ft) thick (Esposito et al., 2008). Sandstone units within the Rodessa Formation are not contiguous, but are collectively referred to as the "Donovan Sand" (Mancini and Puckett, 2002). The Rodessa is sealed by the Ferry Lake Anhydrite, a regionally extensive unit that represents a hiatus in clastic influx to the area. Currently the top of the Rodessa Formation lies 3231-3139 m (10600-10300 ft) below sea level in the study area, sufficiently deep for storage of CO_2 in a supercritical state.

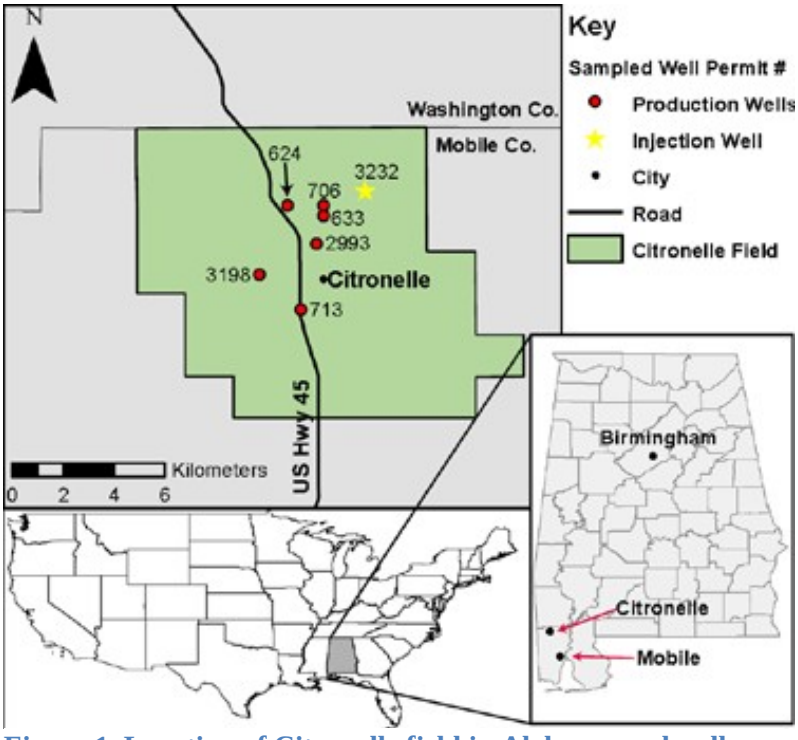

Figure 1. Location of Citronelle field in Alabama and wells used in this study.

The Donovan Sandstone in the Rodessa Formation of the Citronelle Oil Field was targeted for a U.S. Department of Energy CO_2-EOR test. Since drilling began in the Citronelle field in 1955, 169 million bbl of 42-46°

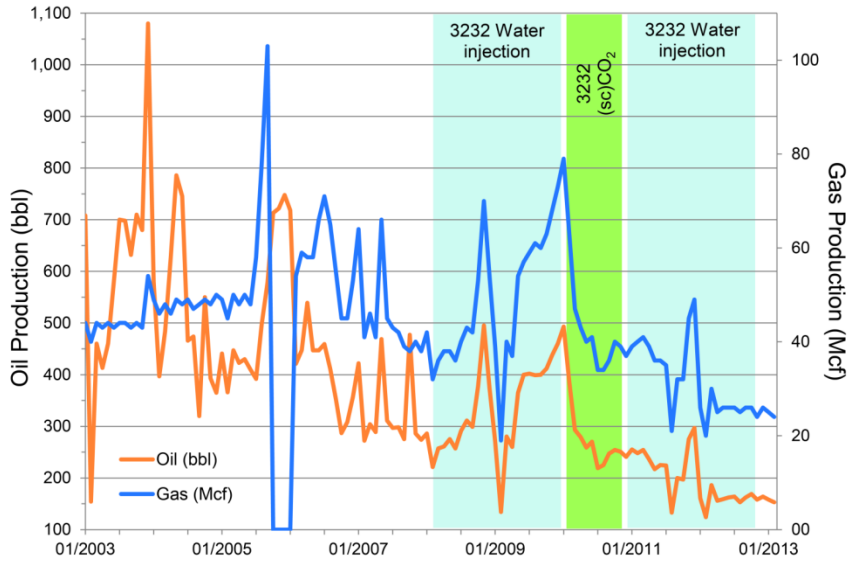

Figure 2. Oil production from OGB Permit 706.

API gravity oil has been extracted from the upper and lower Donovan Sandstone of the Lower Cretaceous Rodessa Formation (Esposito, 2010). An additional 80 million bbl was estimated to be recoverable as a result of CO_2 injection (Esposito, 2010). Well Permit 3232 was transitioned from a producing well to an injection well in 2008. Injection of a 7500 ton slug of food-grade CO_2 began in Permit 3232 in early 2010, followed by water flooding from late 2010 to mid-2012. Oil production from OGB Permit 706 peaked at 493 bbl/month immediately before CO_2 injection, and decreased to well below pre-injection rates after a lower, temporary peak in late 2011 (**Figure 2**).Water-flood injection rates have also decreased since CO_2 injection began.

PERSONNEL INFORMATION & STUDENT TRAINING

Dr. Amy Weislogel served as P.I. of the project in collaboration with co-P.I. Dr. Rona Donahoe. This project supported training of three M.S. students, one graduate research assistant, and six undergraduate students at WVU and UA. The students at WVU were trained in petrographic evaluation of reservoir rock thin-section samples using a petrographic microscopic and SEM imaging, as well as and photomicrograph mapping using Adobe Photoshop, Adobe Illustrator and Nikon Elements software. The students at UA were trained in fluid sample collection, sample analysis and geochemical modeling.

RESULTS OF WORK ON PROJECT TASKS

The project was carried out over three phases as a cooperative effort between Dr. Amy Weislogel of West Virginia University (WVU) and Dr. Rona Donahoe of the University of Alabama (UA). During Phase 1 (1/1/10-12/31/10), reservoir rock samples were obtained from sediment cores and reservoir fluid samples were collected from the wellhead of 4 wells surrounding the injection well. Petrographic and geochemical analyses of reservoir rock samples and initial geochemical analysis of formation fluid was

carried out in Phase 1, including analyses by inductively coupled plasma optical emission spectroscopy (ICP-OES), ion chromatography (IC), and inductively coupled plasma mass spectroscopy (ICP-MS). During Phase 2 (1/1/11-12/31/11) additional petrographic and geochemical analyses of core samples was completed along with more detailed scanning electron microscopy (SEM) imaging and x-ray fluorescence (XRF) analyses of selected core samples. Additional formation fluid samples were collected during and after CO_2 injection to assess the compositional changes induced in formation fluids over time. During Phase 3 (1/1/12-1/31/13), fluid and rock chemistry analyses were finalized and the results combined to determine mineral phases involved in reactive transport processes in order to evaluate the ability of TOUGH2/ECON and TOUGHREACT to simulate the effect of CO_2 injection on reservoir fluid and solid phase geochemistry will be evaluated by comparison of model predictions with fluid geochemistry.

Task 1.0: Project Management and Planning.

The P.I.s post digital technical reports generated for the project and abstracts that have been published or accepted for publication to the project website (https://sites.google.com/site/citronellefluidrockproject/). Outreach and education materials generated for Task 6.0 of our proposal will remain available through this site.

Task 2.0: Reservoir Rock Geochemical Characterization.

Methods

Pre- injection thin–sectioned core samples were analyzed from injection well OGB permit-3232 and six wells up-hydraulic gradient (**Figure 1**): permits 706, 624, 633, 2993, 3198, and 713. Thin-sections were analyzed for framework grain modal composition, grain size and packing geometry, pore type and distribution, and cement composition and distribution. Sample depths ranged from 3,295-3,495 m (10,810-11,466 ft.) depth below mean sea-level. Samples were selected from well cores in order to represent the variety of facies present in each core. Core and core chip samples were analyzed for grain size, sorting, sedimentary structures and fossils, pyrobitumen content, and depofacies. Core chips from an additional two wells, permits 3086 and 3054, were analyzed for lithology, cement composition, presence of hydrocarbons and concretions, and generalized stratigraphy. Mineralogy and porosity from samples in hydrocarbon-producing intervals were obtained by point counting 400 points per sample using a PETROG® Stage Stepper and PetrogLite® software. Grain size minima and maxima measurements were made on the long and short axes of 100 randomly-selected grains over the entire thin section of each sample using Nikon NIS-Elements BR 3.2

Table 1. Sediment texture, cement and porosity attributes of Donovan sandstone samples.

Porosity Types	Grain size (mm)	Grain Packing	Pore Size (mm)	Authigenic Minerals	Cement	Dead Hydrocarbon
High Primary	0.05-0.2	Moderate to Well	0.01-0.05	Hematite	N/A	Prevalent
High Secondary	0.25-0.4	Moderate	0.1-1.0	Calcite	Calcite	Prevalent in primary pores
Mixed Primary and Secondary	0.05-0.5	Moderate	0.01-1.0	Calcite, Anhydrite	Hematite, Calcite, Anhydrite	Prevalent in primary pores
Low Primary	0.01-0.05	Moderate to Poor	0.01-0.05	Hematite, Calcite, Anhydrite	Calcite	Rare

software. Pore area was calculated from photomicrographs using Nikon NIS-Elements BR 3.2 software for 200-400 pore spaces per sample, with secondary dissolution pores distinguished from primary intergranular pores. Porosity determined from thin-section measurement was then compared to porosity values, calculated from bulk density (RHOB) logs in Coffindaffer (2012). Elemental composition of framework feldspars and cements was obtained via Energy Dispersive Spectroscopy (EDS) on polished thin-sections coated with Au-Pd and analyzed using a Hitachi S-4700 field emission scanning electron microscope at 20 kV with a 12 mm working distance.

Reservoir textural properties

Textural properties of Donovan Sandstone samples are given in **Table 1.** Donovan Sandstone reservoir rock is generally fine- to medium-grained and moderately-well to moderately sorted. Maximum grain-size ranges from 1.5 - 0.64 mm and minimum grain-size ranges from 0.08 - 0.05 mm. The mean aspect ratio of grain long axis/short axis was determined for Well 3232 as 1.75 and for Well 706 as 1.98. Grain packing ranges from very loosely packed to tightly-packed; Samples with high cement of any mineralogy are loosely or moderately packed, and samples that are tightly packed are generally cement-poor. However, the inverse relationship is not always true, as some samples with little cement are loosely packed, and these lithologies typically form the main reservoirs. As observed from thin-section, grain packing is consistently loose in conglomerates and vertically-adjacent sandstones. Primary pores are the most commonly observed pore type in the samples, though many samples have significant secondary pores along with primary pores (**Figure 3**). Secondary porosity is most common in samples with low or moderate amounts of cement. Porosity trends **(Figure 4**), derived from bulk density calculated from SP logs (Coffindaffer, 2012), indicate porosity in the Rodessa is highly variable, but the porosity log is consistent with porous (2-5%) thin-sections collected at 3338 m (10950 ft) and 3364 m (11038 ft). Porosity and pore area exhibit a strong positive correlation for well 3232 and well 706 ($r = 0.84$ and $r = 0.98$ respectively). Porosity and grain size are also

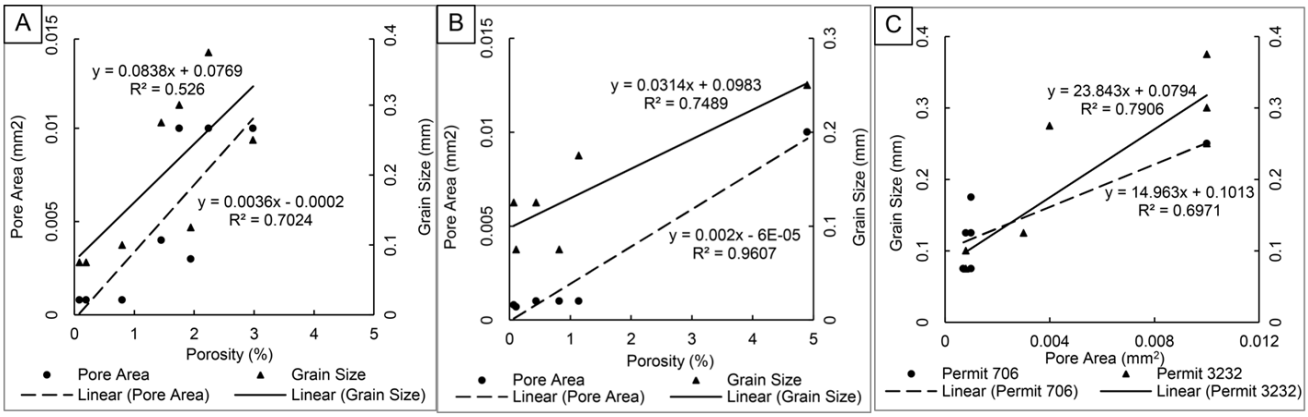

Figure 3. Porosity vs. average pore area and average grain size, for (A) well permit 3232 and (B) permit 706. (C) Average pore area vs. average grain size for wells 3232 and 706.

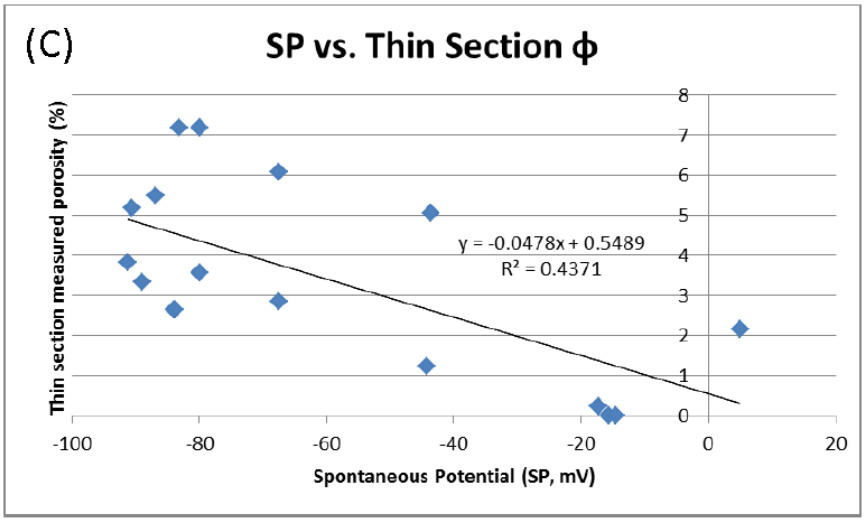

Figure 4. Cross-plot of SP log values for sandstone units compared to thin-section porosity measurements of samples from wells 3232 and 706.

positively correlated for wells 3232 and 706 at r = 0.73 and r = 0.87, respectively (**Figure 3**). Pore area and grain size are also strongly positively correlated for well 3232 and well 706 at r = 0.89 and r = 0.83 respectively. Conglomerates are an exception to this trend, as they are entirely cemented and have virtually no porosity.

Reservoir compositional properties.

Sand mineralogy is uniformly arkosic (**Figure 5**); even so, original feldspar content was likely higher, as secondary pore spaces inporous samples were generated from alteration and dissolution of detrital feldspar grains. Feldspar grains analyzed by EDS suggest a slightly greater abundance of plagioclase over orthoclase. Pure-Na or Na-rich feldspar is the dominant form of plagioclase and there is no apparent relationship between Na content and plagioclase alteration and dissolution. In contrast to framework grain mineralogy, authigenic mineralogy and porosity are highly heterogeneous (**Table 1**).

Feldspar alteration and replacement is common. Calcite is the dominant replacement mineral, though in rare cases anhydrite, possibly after calcite, is observed to replacing albite. Partial and complete feldspar dissolution is also common, forming much of the reservoir's secondary porosity. Reservoir sandstone samples typically exhibit open framework-grain packing. This packing arrangement was preserved by early calcite cementation. Original porosity averages, estimated from measurements of pore area plus pyrobitumen area, are ~4%, but locally samples exhibit >10% porosity. Pore sizes are also typically bimodal, consisting of smaller primary pores and larger secondary pores. Pore size distribution in high porosity reservoir rock is often bimodal due to the presence of both smaller primary pores and larger secondary pores.

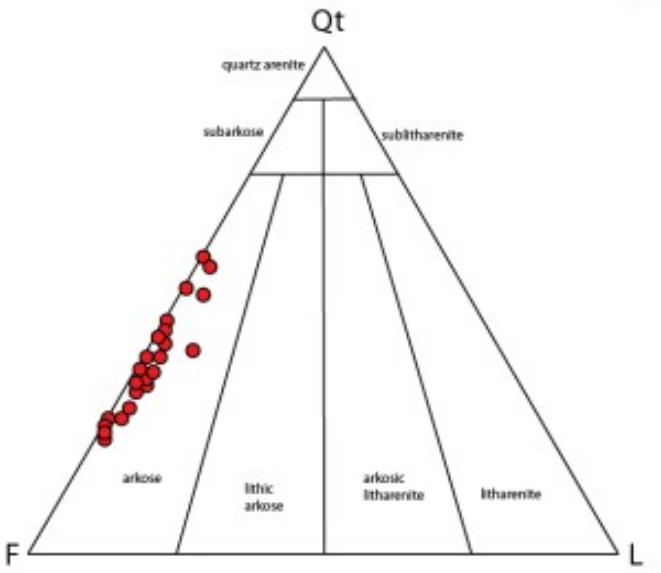

Figure 5. Modal abundance of sandstone framework grain components. Qt = total quartz grains, F = total feldspar grains, L = lithic grains, not including polycrystalline quartz.

Diagenetic processes caused depletion of unstable phases such as feldspar from sandstone (McLennan et al., 1993; Nesbitt and Young, 1984; Nesbitt et al., 1996). Nesbitt and Young (1984) formulated the Chemical Index of Alteration (CIA) based on abundances of mobile cations found in unstable framework grains relative to less mobile cations found in more refractory phases to assess weathering intensity:

$$CIA = Al_2O_3/(Al_2O_3+CaO^*+Na_2O+K_2O)$$

where all components are compared as molar proportions, and CaO* is equal to Ca contained only in the silicate fraction (i.e., excludes Ca derived from carbonate). Calculation of CaO* follows the method outlined in Fedo et al. (1995). Results indicate that CIA for most samples suggests an abundance of immobile Al_2O_3 for most samples, but that some lithologies suggest increased CaO, Na_2O and/or K_2O (**Figure 7**). Lithologies with low CIA values are likely zones that either did not experience significant feldspar dissolution, or in which secondary pores were later filled with calcite. If conditions favoring dissolution were to affect these lithologies, new pore networks could develop in previously tight rock.

Reservoir diagenetic history.

The post-depositional chemical changes to the reservoir rock can be outlined in the following paragenetic sequence:

Stage 1. Poikilitopic calcite cementation and feldspar alteration: The poikilitopic texture observed in calcite-cemented samples resulted from very early diagenetic processes operating shortly after deposition and before significant burial and compaction of framework grains, as samples with abundant poikilitopic cement exhibit loose grain packing. Such cementation occurred in a shallow, marine or brackish phreatic zone with sufficient calcium and bicarbonate for calcite precipitation. The phreatic zone was characterized by very high sediment permeability and interstitial fluid flow rates, and relatively slow burial/subsidence. This is consistent with relatively low subsidence rates during the Cretaceous (<100 m/million years; Pashin et al., 2007). This early calcite cementation filled most primary porosity in the Donovan Sandstone, and samples with high secondary porosity, loose grain packing, and moderate-high pyrobitumen content are interpreted to have originally been calcite-cemented, with cement being mostly dissolved later in the paragenetic evolution, prior to hydrocarbon charging. Some tightly-packed intervals lack significant cement and likely developed during periods in which fresh, acidic meteoric water derived either via fluvial transport or groundwater discharge in the delta platform diluted or flushed out the more saline, alkaline water that typically occupied the interstitial pores; this relatively fresh interstitial water prevented phreatic calcite precipitation and enabled subsequent compaction. Such freshwater influx may represent episodes of relatively higher precipitation in the delta drainage system. Altered feldspars are common in virtually every sample, with altered areas replaced by calcite, and less commonly anhydrite, with minor illite, montmorillonite and kaolinite. Widespread feldspar alteration is inferred to have occurred as a result of vigorous, near-surface weathering during deposition, prior to substantial compaction. The lack of significant clay alteration products that result from surface and near-surface feldspar hydrolysis suggests this alteration

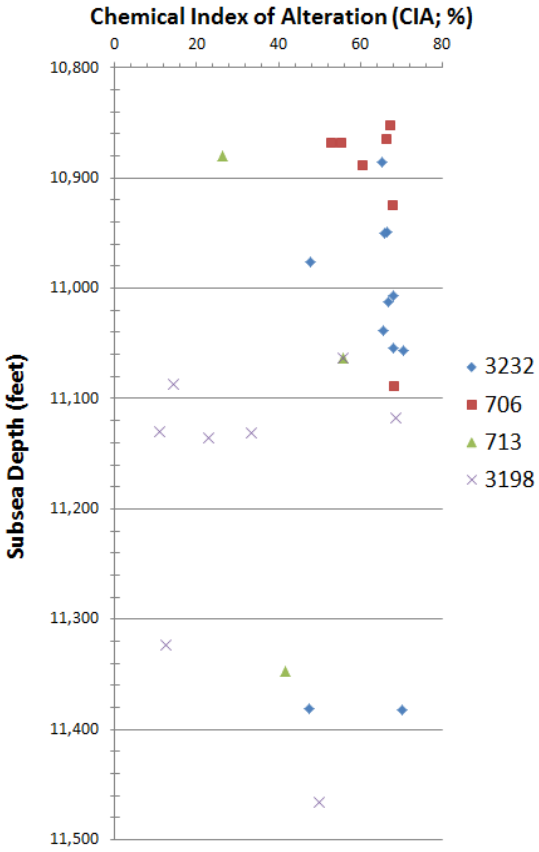

Figure 7. Chemical Index of Alteration results for core samples taken from 4 different wells plotted versus sample depth.

occurred while the interstitial pores formed a system open to through-going fluid. Feldspar alteration continued during later diagenetic stages as reflected by replacement of feldspar by authigenic cements.

Stage 2: Partial dissolution of calcite cement and framework grains. Much of the secondary porosity observed is interpreted to have formed from dissolution of feldspar framework grains. Partial feldspar dissolution is observed to have formed delicate feldspar skeletons (**Figure 8**), suggesting that pore-fluid pressure was at least equal to the lithostatic pressure, thereby preventing collapse and destruction of the grain. Secondary pores would not have survived initial burial and compaction if dissolution occurred early in diagenesis. Infilling of partially-dissolved feldspars by pyrobitumen suggests that hydrocarbon charging occurred coeval with or shortly subsequent to feldspar dissolution. However, the presence of empty secondary pore space that lack pyrobitumen suggests that either such pores contained fluid hydrocarbons which have been removed by oil production, or that feldspar dissolution continued after hydrocarbon charging. We propose that feldspar dissolution occurred during Based on the burial, subsidence and hydrocarbon maturation curves (Pashin et al., 2007), the Smackover Formation source rock was in the gas generation stage by the time the Donovan Sand reached maximum depth in the early Tertiary. Such late-stage maturation would supply the CO_2 necessary for feldspar dissolution during hydrocarbon charging. Siebert et al. (1984) concluded that partial and complete feldspar dissolution often occurs later in diagenesis or at least after initial cementation as acidified fluids associated with hydrocarbon source expulsion, and subsequent dewatering of the source shale which are capable of feldspar dissolution, forming aluminum-organic complexes that are flushed out of the reservoir. They suggest methane as the driving pressure in fluid migration during this process.

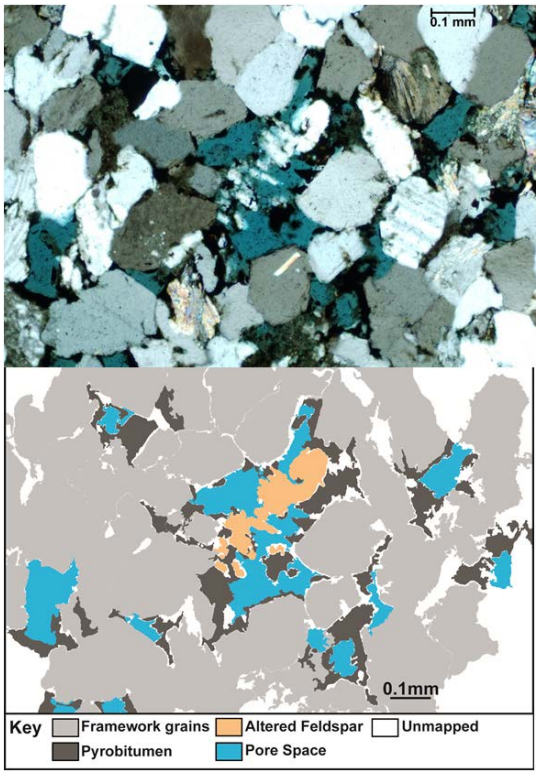

Figure 8. Photomicrograph showing skeletal remains of a feldspar grain. Blue-dyed epoxy fills pore spaces and dark areas represent pore spaces filled with pyrobitumen.

Stage 3: Secondary calcite cementation, formation of calcite and anhydrite concretions, and dolomitization. Re-precipitation of dissolved calcite in secondary pores is inferred where cement occupies regions larger than the average grain size of the sample. Re-precipitation may have occurred concurrently with calcite dissolution in other areas of the formation, though this is difficult to constrain. This phase of calcite cementation was localized, and not pervasive throughout the entire formation, as is evidenced by the preservation of secondary porosity in many samples. Dolomite-rich samples are generally pyrobitumen-poor to barren, but where present, pyrobitumen is visible as infill between dolomite crystals, indicating a pre-charge timing of dolomitization. Calcite and anhydrite concretions formed in some samples, likely immediately preceding or synchronous with hydrocarbon charge, such that SO_4^{-2} associated with hydrocarbon emplacement was available to drive the precipitation of anhydrite (**Figure 9**). Heydari and Moore (1989) also report late anhydrite formation in the Smackover Formation source rock prior to hydrocarbon migration. It is unclear if the calcite concretions formed indirectly from incomplete dissolution of the surrounding cement, or if they represent another phase of cement formation.

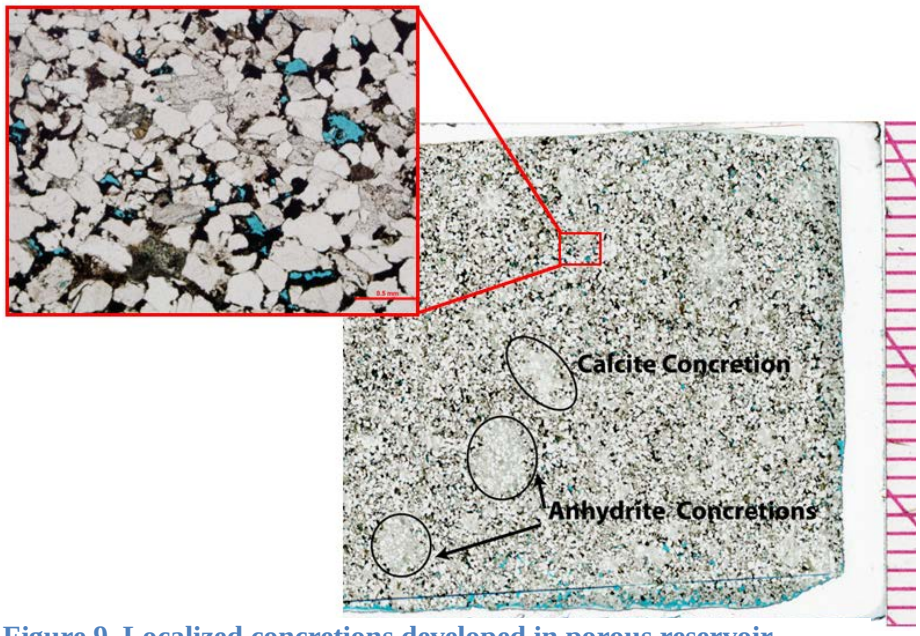

Figure 9. Localized concretions developed in porous reservoir sandstone.

Figure 10. Core showing oil-stained sandstone on the left with calcite and anhydrite concretions in the upper-right hand core.

Stage 4: Hydrocarbon charging. Porous intervals of the Donovan Sand exhibit hydrocarbon staining (**Figure 10).** Hydrocarbon charging occurred late in the paragenetic history,

after formation of secondary porosity through framework grain and cement dissolution, as well as dolomitization. Exact timing of charging is beyond the scope of this study; however, feldspar dissolution due to mature hydrocarbon-sourced CO_2 would suggest that hydrocarbon charge occurred when the Smackover entered its main gas generation phase in the late Cretaceous to early Tertiary (Pashin et al., 2007).

Stage 5: Pyrobitumen formation. Further heating of the hydrocarbons resulted in pyrobitumen formation. It is inferred to be the last stage, as many secondary pores are partially-filled by pyrobitumen and contain no other cements. The exact timing of pyrobitumen development is uncertain, but can be inferred to have occurred in the late Tertiary, as the Rodessa Formation entered the late hydrocarbon maturation window reported by Pashin et al. (2007).

Summary. Study of the diagenetic history of the Donovan Sand reservoir indicates that carbonate cementation and feldspar dissolution variably occurred during diagenesis resulting in heterogeneous composition of intergranular material within the reservoir rock, and alteration of framework grains, intergranular cementation, and dissolution of intergranular cement served as the main control on primary and secondary porosity development. Early cementation destroyed primary porosity in some intervals, whereas in other places early cement provided the framework for secondary pores developed due to feldspar dissolution produced porosity. We hypothesize that carbonic and sulfuric acid associated with hydrocarbon charging aided in dissolution of feldspar and possibly any clay weathering products. These results indicate that miscible-CO_2 interactions with formation water and reservoir rock can create similarly acidic formations water chemistry capable of causing short- and long-term changes in formation matrix geochemistry and permeability, thereby affecting the long-term CO_2 storage capacity and EOR production of the reservoir. The removal of hydrocarbons from grain surfaces during EOR may lead to continued secondary porosity development via acidic or acidified formation waters, thus in essence making the diageneitc history of Donovan sandstone a predictive analog for future rock-fluid interactions. We interpret that the heterogeneity of the Donovan Sand developed from polyphase mineral precipitation and dissolution in the reservoir matrix during diagenesis is likely responsible for forming preferential flow paths within high porosity zones of the reservoir matrix. Viscous fingering of CO_2 due to differential flow along theses paths could have resulted in the initial increase and subsequent decline in CO_2 -EOR of the Donovan Sandstone.

Task 3.0: Fluid Geochemistry.

Water samples were collected from producing wells B-19-7, B-19-8, B-19-9 and B-19-11 in the Citronelle oil field were analyzed by ICP-OES for major cations, by ICP-OES with matrix matching for trace elements, and by ion chromatography for anions. Small volume titrations (0.8 ml) were also conducted using a gas bench, to determine alkalinity values. These results suggested that the oxidation of organic constituents of crude oil contributed to the CO_2 stream measured at the detector of the gas bench mass spectrometer. Therefore, CO_2 values derived from this experiment likely reflect total dissolved organic carbon and total dissolved inorganic carbon, rather than only total inorganic carbon, which could be used to derive sample alkalinity. Dionex OnGuard II RP hydrocarbon filters were used to remove organic constituents of the water samples, and the gas bench analyses were repeated. However, the carbon measurements appear to have been compromised, either by contaminants contained in the filters or by the introduction of particulate matter contained in the hydrocarbon filters. Mineral saturation indices (SI) were calculated for water samples using the PHREEQC.out macro developed for this project. Mineral saturation indices were calculated in order to determine potential mineral sources and sinks for the aqueous elements and temporal plots were created to show changes in water chemistry with time for each of the monitoring wells. The influence of CO_2 injection on lowering the pore water pH is clearly seen over the first 250 days of the monitoring period (**Figure 11**). Well B-19-11 was shut in for approximately 8 months due to overpressuring and pump damage, so this trend cannot be seen in

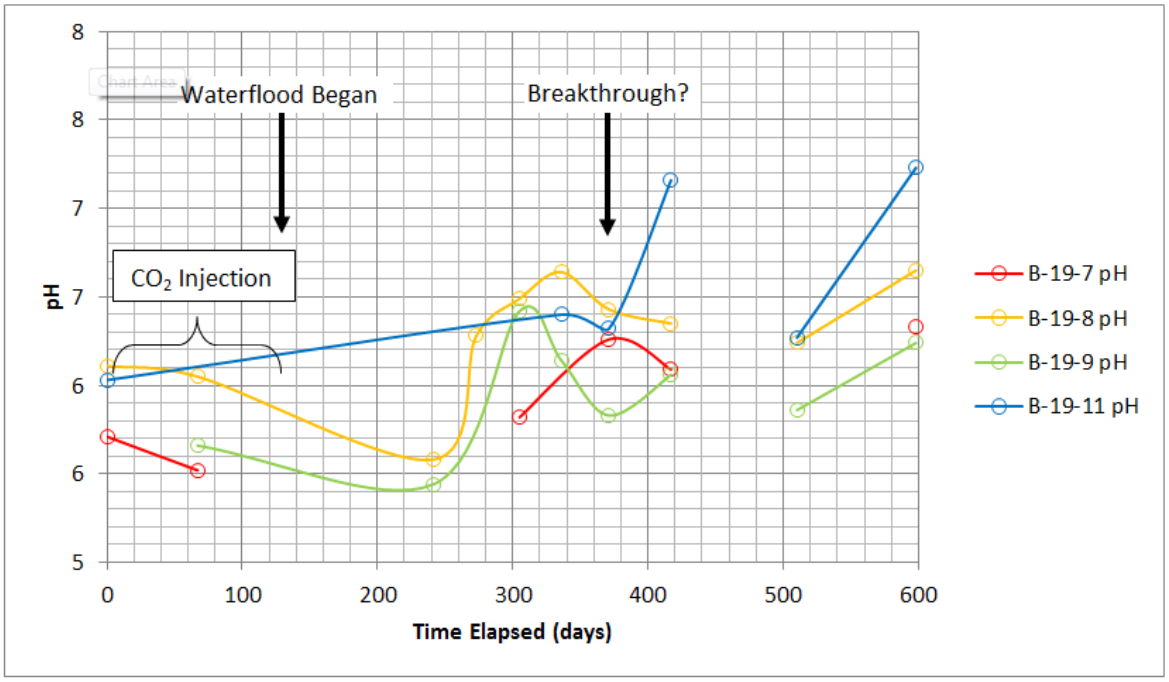

Figure 11. Aqueous pore fluid pH as a function of time for wells B-19-7, B-19-8, B-19-9 and B-19-11.

data from that well.

Although CO_2 injection ended and waterflood began in October 2010, reservoir pore fluid pH did not increase until after February 2011. It appears that Well B-19-11, which was the first well to show CO_2 breakthrough, also experienced injection water breakthrough first, as evidenced by an increase in pore fluid pH in February 2012. Breakthrough of injection water in Well B-19-11 is also indicated by a large decrease in aqueous Fe concentration (**Figure 12**). Both pH and Fe concentrations in Well B-19-8 suggest that this well will be the next to show injection water breakthrough. Several pore fluid parameters suggest that Well B-19-11 and Well B-19-8 are more hydraulically and geochemically connected, while Well B-18-7 and Well B-19-9 are more alike and less connected hydraulically to the other two wells. This is illustrated by pore fluid Ba concentrations, shown in **Figure 13**.

For individual wells, Ca-Sr concentrations (**Figure 14**) and Ba-Mn concentrations (**Figure 12**) are highly correlated. Calcium, Ba and Sr are all alkaline earth elements and tend to track together due to their geochemical similarity. Mn can also exist in solution as a divalent cation. The temporal trends of all four elements are quite similar for Well B-19-9. Significant increases in the concentrations of several elements (e.g., Ba, Ca, Fe, Mn, Sr) were observed for all wells between February and March/April of 2011. This cannot be seen for Well B-19-11 because samples could not be collected during the shut-in

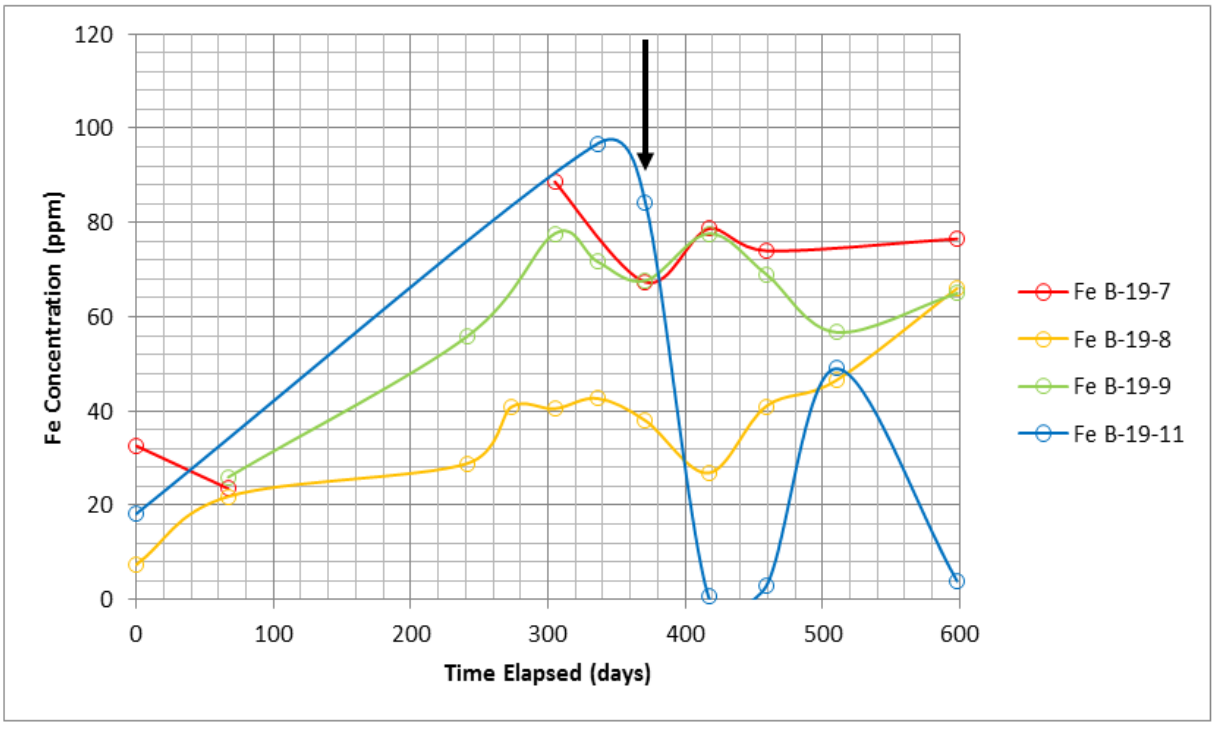

Figure 12. Aqueous pore fluid Fe concentration as a function of time for wells B-19-7, B-19-8, B-19-9 and B-19-11.

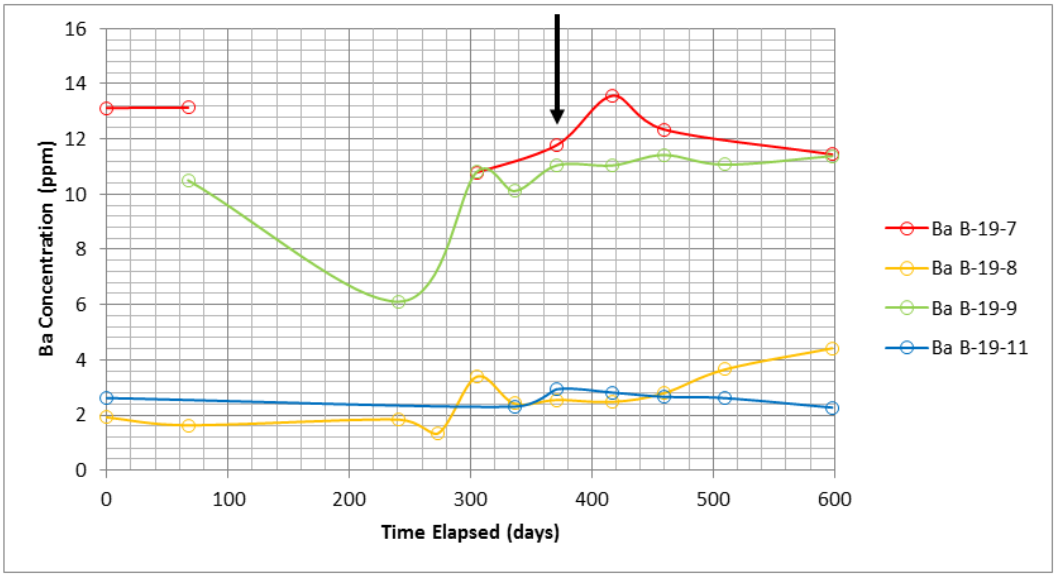

Figure 13. Aqueous pore fluid Ba concentration as a function of time for wells B-19-7, B-19-8, B-19-9 and B-19-11.

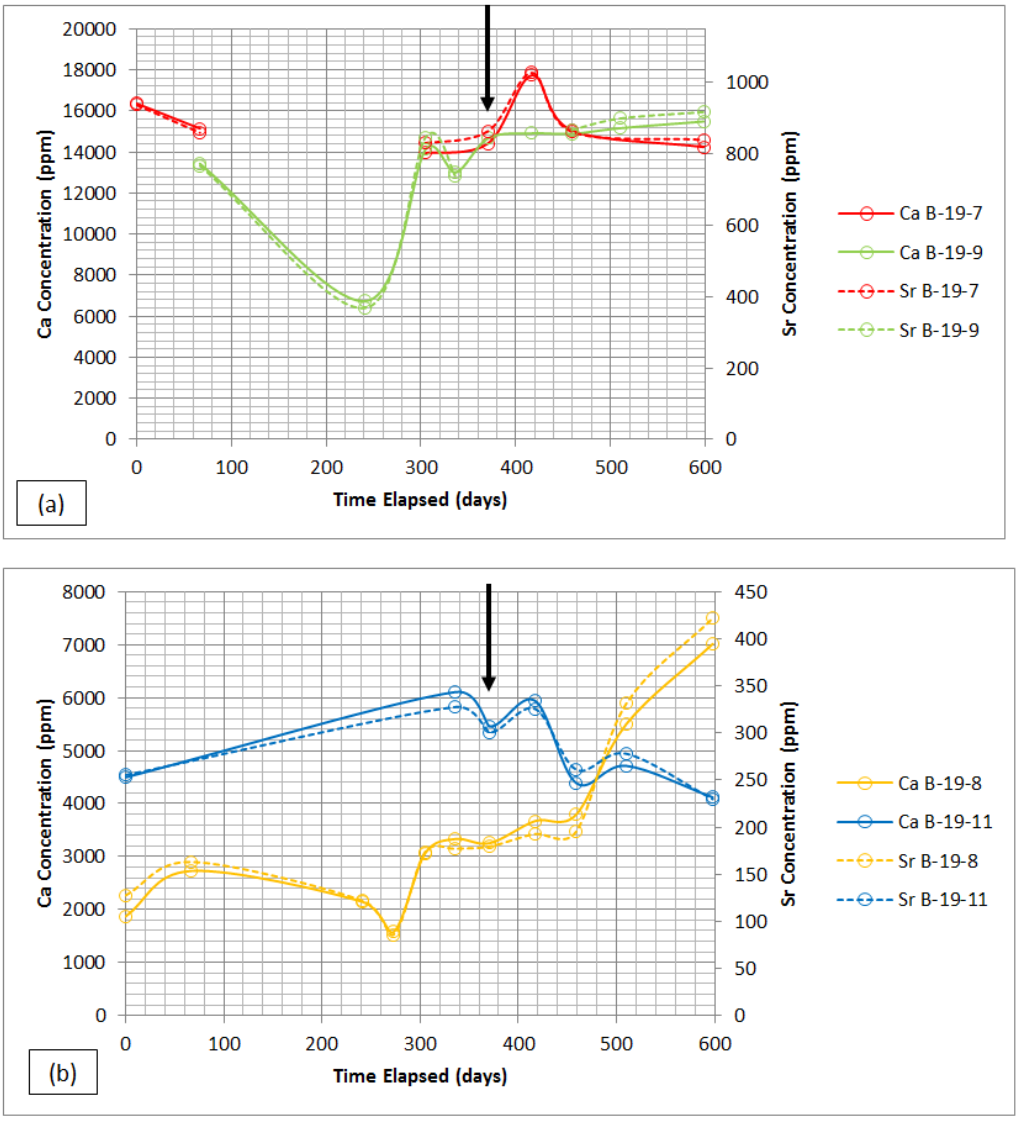

Figure 14. Aqueous pore fluid Ba and Mn concentrations as a function of time (a) for wells B-19-7 and B-19-9 (b) for wells B-19-8 and B-19-11.

Table 2. Temporal changes in mineral saturation indices at 110°C as determined by PHREEQC

	Day	Ionic	Albite	Anorthite	Quartz	Muscovite	Anhydrite	Calcite	Dolomite	Hematite	Fe(OH)3	Smectite-high-Fe-Mg
B-19-7 110C	0	3.37	-0.49	-2.34	-0.52	2.82	-0.21	0.92	2.54	21.05	5.53	-1.34
	67	3.51	-1.05	-2.57	-0.74	2.97	-0.45	0.74	2.19	20.41	5.20	-2.36
	241											
	273	2.97	0.23	-1.85	-0.28	3.71	0.06	0.82	2.32	21.59	5.80	-0.40
	305	2.79	-0.08	-2.14	-0.36	2.93	-0.10	0.97	2.64	22.01	6.02	-0.47
	336											
	371	2.98	-0.19	-2.22	-0.40	1.93	0.04	1.36	3.42	22.54	6.28	-0.03
	417	3.46	1.27	0.28	-0.32	6.04	0.10	1.26	3.23	22.46	6.23	1.66
	459	3.00	N/A	N/A	N/A	N/A	1.66	2.23	3.49	N/A	N/A	N/A
	510											
	598	2.52	0.33	-1.40	-0.32	3.10	-0.10	1.37	3.46	22.70	6.37	0.82

	Day	Ionic	Albite	Anorthite	Quartz	Muscovite	Anhydrite	Calcite	Dolomite	Hematite	Fe(OH)3	Smectite-high-Fe-Mg
B-19-8 110C	0	0.34	-0.34	-2.25	-0.21	2.65	-0.38	0.84	2.33	20.26	5.19	-1.22
	67	0.59	0.04	-2.04	-0.12	3.01	0.02	0.83	2.27	21.10	5.60	-0.62
	241	0.42	-0.29	-2.41	-0.19	3.33	-0.12	0.33	1.23	20.55	5.33	-1.74
	273	0.31	-0.16	-2.03	-0.17	2.59	-0.05	0.94	2.40	21.98	6.05	-0.47
	305	0.45	-0.38	-2.19	-0.24	1.77	-0.25	1.29	3.19	22.21	6.16	-0.14
	336	0.73	0.21	-1.89	-0.11	2.03	0.13	1.40	3.37	22.41	6.25	0.49
	371	0.54	0.17	-1.92	-0.11	2.48	-0.11	1.23	3.04	22.08	6.10	0.22
	417	0.66	0.88	-0.26	-0.18	5.00	0.06	1.18	2.93	21.69	5.90	0.89
	459	0.70	0.09	-1.97	-0.15	1.08	0.01	1.74	4.04	22.62	6.36	0.80
	510	1.04	0.09	-2.11	-0.16		0.04	1.13	2.98	22.04	6.06	
	598	1.30	0.44	-1.65	-0.13	2.22	0.05	1.51	3.75	22.82	6.45	1.20

	Day	Ionic	Albite	Anorthite	Quartz	Muscovite	Anhydrite	Calcite	Dolomite	Hematite	Fe(OH)3	Smectite-high-Fe-Mg
B-19-9 110C	0											
	67	3.06	-0.38	-2.33	-0.45	3.06	-0.02	0.84	2.38	20.74	5.38	-1.37
	241	1.29	-0.84	-2.72	-0.49	2.96	-0.38	-0.44	-0.24	19.88	4.98	-2.54
	273											
	305	2.60	0.29	-1.78	-0.26	2.28	-0.18	1.48	3.66	22.83	6.43	0.83
	336	2.62	0.41	-1.40	-0.29	3.28	0.00	1.24	3.16	22.39	6.21	0.51
	371	2.97	0.44	-1.68	-0.23	3.56	0.04	1.00	2.68	21.84	5.93	0.07
	417	2.90	-0.31	-2.98	-0.27	1.25	0.05	1.20	3.10	22.36	6.19	-0.40
	459	3.06	-0.02	-2.21	-0.32	0.47	0.12	1.88	4.46	23.25	6.63	1.12
	510	2.97	0.25	-1.93	-0.25	N/A	0.14	1.00	2.71	21.75	5.89	
	598	2.89	0.28	-1.91	-0.24	2.49	0.12	1.33	3.36	22.47	6.25	0.55

	Day	Ionic	Albite	Anorthite	Quartz	Muscovite	Anhydrite	Calcite	Dolomite	Hematite	Fe(OH)3	Smectite-high-Fe-Mg
B-19-11 110C	0	0.83	-0.28	-2.18	-0.32	2.84	-0.30	0.92	2.54	20.91	5.50	-0.94
	67											
	241											
	273											
	305											
	336	1.38	0.46	-1.64	-0.16	2.64	-0.22	1.25	3.45	22.90	6.49	1.13
	371	1.22	0.30	-1.98	-0.14	2.58	-0.09	1.16	3.22	22.67	6.38	0.76
	417	1.30	-0.69	-2.97	-0.40	-0.46	-0.22	1.93	4.83	18.99	4.53	-0.89
	459	0.90	-0.44	-2.54	-0.35	0.48	-0.48	1.77	4.45	20.31	5.20	-0.31
	510	1.05	0.02	-2.26	-0.18		-0.13	1.10	3.09	22.13	6.11	
	598	0.82	-0.28	-2.31	-0.30	0.35	-0.21	1.94	4.72	20.68	5.39	0.19

period. In the same time period, pore fluid pH also increased (**Figure 15)**. These trends could indicate that mineral dissolution reactions, cation exchange reactions, or a combination of the two is responsible for the observed trends. Mineral saturation indices calculated for 110° C are shown in **Table 2**. `

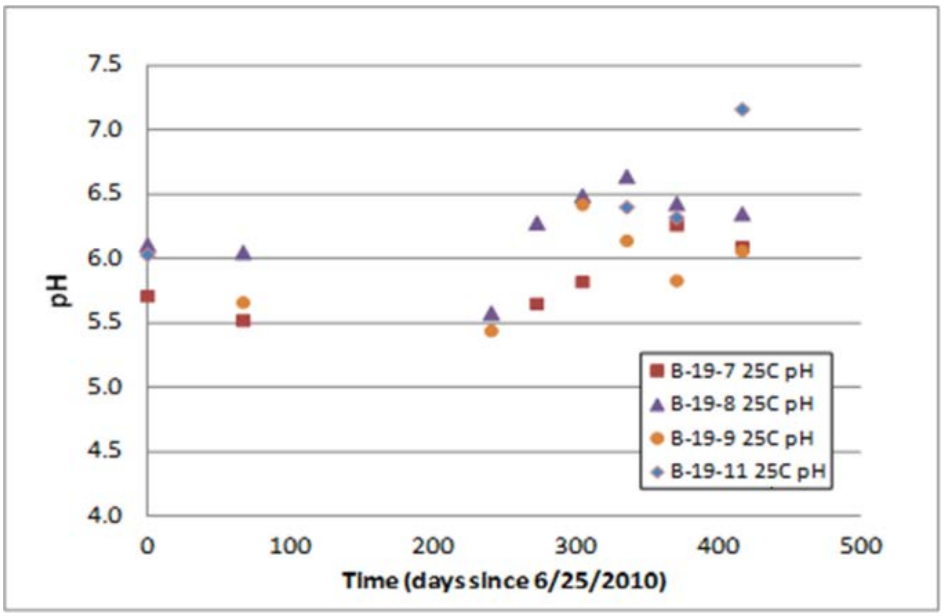

Figure 15. Results from PHREEQC and PHREEQPITZ modeling for pH, Mineral Saturation Indices and Fe concentration.

The SI values for minerals present in the reservoir rock do not indicate mineral dissolution reactions that could explain the observed element concentration trends. It therefore appears more likely that ion exchange reactions between H+ sourced from carbonic acid generated by the injection of supercritical CO_2 and cations on the surfaces of reservoir minerals are responsible for the observed element concentration trends. The SI values for minerals present in the reservoir rock do not indicate mineral dissolution reactions that could explain the observed element concentration trends.

Task 4.0: Geochemical Modeling.

TOUGH family models allow modeling of multiphase fluid flow under pressure, viscous and gravitational forces, simulation of fluid/rock interactions, heat flow and diffusion. TOUGHREACT was evaluated as a tool for modeling mineral-fluid reactions induced by super critical CO_2 injection into an oilfield brine, followed by waterflood. A rastered map of the Citronelle oil field was used to determine well locations on a Cartesian coordinate grid and the distance between the injector and monitoring wells (**Figure 16**). Locations of the injection well and

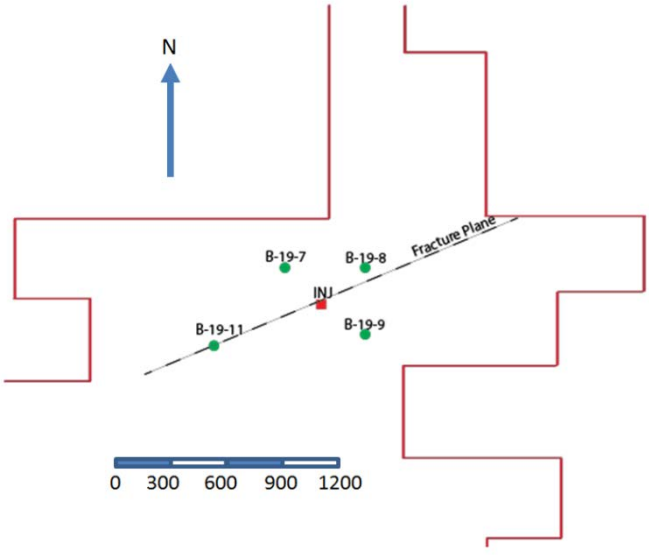

Figure 16. Well locations and proposed trend for vertical fracture plane.

Table 3. Cartesian coordinates for TOUGHREACT modeling.

Well	X (px)	Y (px)	X (m)	Y (m)	Distance (m)
top_left	0	0	12.5	12.5	----------
INJ	388	206	787.5	412.5	0
B-19-7	295	114	587.5	212.5	265.82
B-19-8	499	116	1012.5	237.5	290.38
B-19-9	499	283	1012.5	587.5	274.51
B-19-11	116	310	237.5	637.5	591.73
bottom_right	700	400	1412.5	812.5	----------

Table 4. Donovan sandstone mineralogical data conversion.

Mineral	Mass %	Density (g/cm^3)	Volume %
Quartz/Silica	36.18%	2.63	36.17%
Plagioclase	2.16%	2.69	2.12%
Orthoclase	45.87%	2.56	47.12%
Sedimentary	2.08%	2.5	2.19%
Muscovite	4.42%	2.83	4.10%
Biotite	0.45%	3.1	0.38%
Calcite	5.35%	2.71	5.19%
Anhydrite	2.55%	2.97	2.26%
Hematite	0.95%	5.3	0.47%

the four monitoring wells are given in **Table 3** and shown in **Figure 16**.

The wells were placed on a finite-difference grid of 25 m spacing for the TOUGH2 physical model. Petrologic data obtained from PI Weislogel's group at WVU were used to input average mineral abundances for the Donovan sandstone into the TOUGHREACT model. This required conversion of point count data in mass % to volume % (**Table 4**), which was accomplished by dividing the mass-density ratio of each mineral by the sum of mass-density ratios of all minerals.

Porosity was initially estimated at 20%, and permeability was estimated to be 10-12 m^2, values typical of oil reservoir sandstones. An average rock density of approximately 2630 kg/m^3 was calculated by summing the products of mineral density and volumetric fraction. Reactive surface area was estimated through assumed average grain sizes and the volume percent of minerals.

Table 5 shows the compilation of kinetic parameters for minerals identified in the Donovan sandstone taken from the TOUGHREACT user's guide. These parameters are described in detail in both the TOUGHREACT user's guide and in a PetraSim tutorial for CO_2 sequestration in TOUGHREACT. Kinetic constraints dictate dissolution and precipitation rates for each mineral and are generally the lowest for silicates and aluminosilicates, and the highest for carbonates and iron minerals. Fluid samples collected for this project showed chemical similarities for wells B-19-11 and B-19-8, with these wells having the lowest sodium concentrations. In contrast, samples collected from wells B-19-7 and B-19-9 were consistently much more saline. We hypothesize that the vertical fracture trends NE-SW, as shown in Figure 16, and hydraulically connects the B-19-10 #2 injection well with wells B-19-8 and B-19-11.

Table 5. Kinetic parameters assumed for reservoir minerals in TOUGHREACT.

	Dissolution and Precipitation Rate		Primary pH-dependent Rate			Secondary pH-dependent Rate		
Mineral	Rate constant (K25)	Ea (kJ/mol)	Weighting Factor k25	Ea (kJ/mol)	n(H+) Exponent	Weighting Factor k25	Ea (kJ/mol)	n(H+) Exponent
quartz	4.30E-14	87.7	2.14E-11	65	0.457			
Amorphous silica	8.84E-13	62.8						-0.572
albite~low	2.75E-13	69.8	6.92E-11	65	0.457	2.51E-16	71	-0.823
k-feldspar	3.89E-13	38	8.71E-11	51.7	0.5	6.31E-22	94.1	
calcite	1.00E-11	41.87						
muscovite	2.40E-14	58.48						
anhydrite	1.50E-12	80						
anorthite	1.50E-12	68.73						
oligoclase	1.45E-13	69.8						-0.472
kaolinite	6.92E-14	22.2	4.90E-12	65.9	0.777	8.91E-18	17.9	-0.4
illite	1.66E-13	35	1.05E-11	23.6	0.34	3.02E-17	58.9	-0.4
smectite-ca	1.66E-13	35	1.05E-11	23.6	0.34	3.02E-17	58.9	-0.4
smectite-na	1.66E-13	35	1.05E-11	23.6	0.34	3.02E-17	58.9	
hematite	2.51E-15	66.2	4.07E-10	66.2	1			
magnesite	4.57E-10	23.5	4.17E-07	14.4	1			
pyrite	4.00E-11	56.9						
siderite-2	1.26E-09	62.76	6.46E-04	36.1	0.5			

A 1D model was instead implemented to describe a preferential flow path between the injection well and pumping well. Linear distances between the injector and observation wells are given in **Table 3**. The 1D model assumed CO_2 saturation and an initial brine composition identical to that of the 6-25-10 sample collected from well B-19-7.

Initial 2D modeling efforts in TOUGHREACT failed to simulate field site observations and failed to produce neither realistic breakthrough times nor reasonable concentrations and temporal trends for water chemistry. After TOUGHREACT model runs failed to converge for high water injection rates, and failed to demonstrate breakthrough for reduced water injection rates, permeability was increased by 2 orders of magnitude, to 10^{-10} m^2. Even nearly infinite permeability estimates did not allow for convergence, and reasonable permeability estimates did not allow for breakthrough of injected water at any of the sampled wells, even after a 100 year simulation. TOUGHREACT predicted Si concentrations which were similar to those observed, but predicted a much larger increase during CO_2

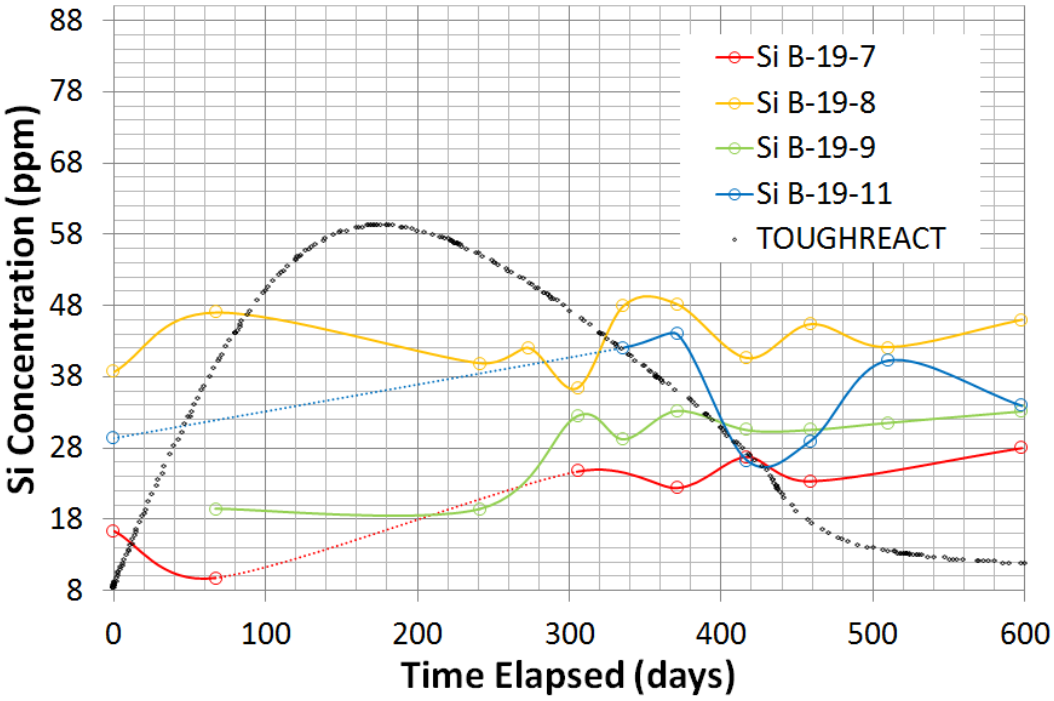

Figure 17. TOUGHREACT predicted Si concentrations which were similar to those observed, but predicted a much larger increase during CO2 injection and decrease during waterflood than was observed in any of the wells.

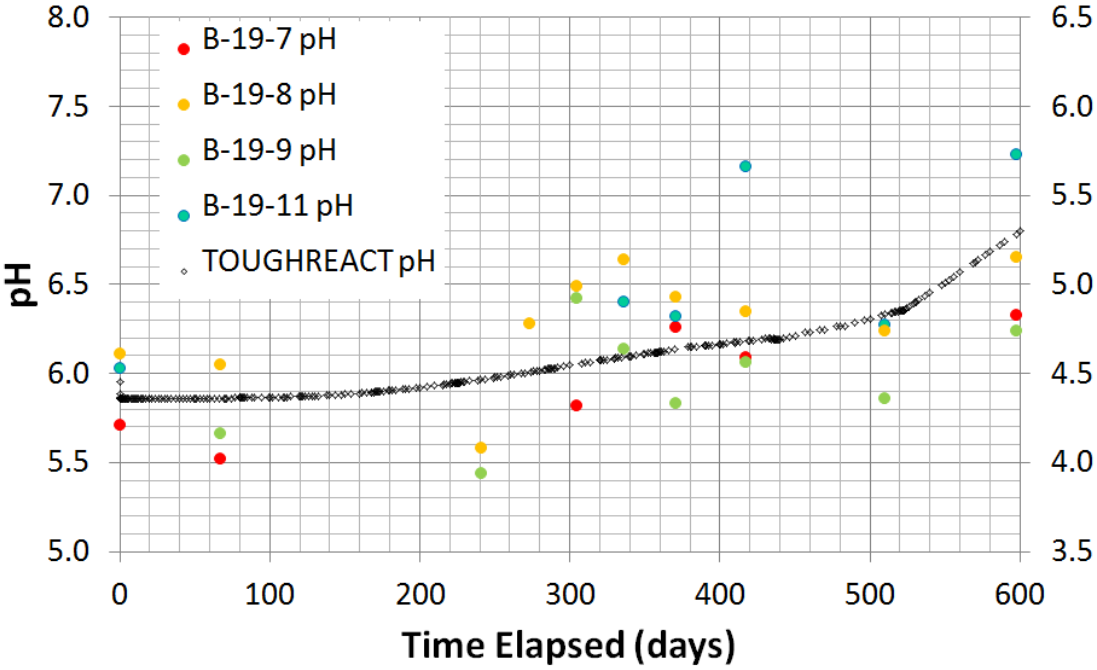

Figure 18. The pH trend calculated by TOUGHREACT showed broad correspondence to the observed pH data; however, note that the finite pH values predicted were approximately 1.5 pH units lower than the observed values

injection and decrease during waterflood than was observed in any of the wells (**Figure 17**). Although the pH trend calculated by TOUGHREACT showed broad correspondence to the observed pH data, note that the finite pH values predicted were approximately 1.5 pH units lower than the observed values (**Figure 18**). TOUGHREACT predicted a loss of $CaCO_3$ after 1 year. However, the change in

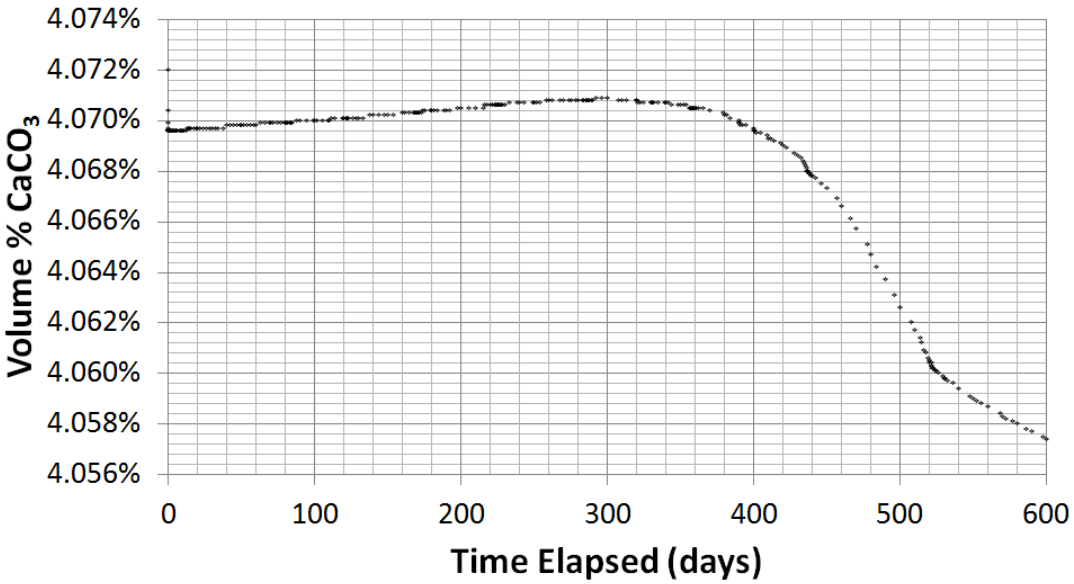

Figure 19. TOUGHREACT predicted a loss of CaCO3 after 1 year. However, the change in % CaCO3 predicted was tiny (<.02%) and is not supported by calcite saturation index calculations for the collected samples.

% $CaCO_3$ predicted was tiny (<.02%) and is not supported by calcite saturation index calculations for the collected samples (**Figure 19**).

A pressure-transient test performed in November and December of 2011 by Walsh et al. (DE-FC26-06NT43029) provided strong evidence that a 600-1000 foot vertical fracture intersects the injection well. The Donovan sandstone is free of natural fractures; therefore the vertical fracture was likely the result of accidental hydraulic fracturing of the hydrocarbon-bearing sand units during initial difficulties with CO_2 injection. This fracture explains the early, excessive breakthrough of CO_2 and loss of oil production in well B-19-11 as well as chemical data collected for this study.

Task 6.0 - Outreach and Technology Transfer

Results from this project were presented by project PI and co-PI as well as student research assistants at 10 conferences including the Annual Conference on Carbon Capture Utilization & Sequestration, DOE-NETL Carbon Storage R&D Project Review, Geological Society of America Annual Meeting, Northeastern Section of the Geological Society of America Annual Meeting, American Association of Petroleum Geologists, and Southeastern Section of the American Association of Petroleum Geologists. Project quarterly reports and abstracts are archived on our project website (https://sites.google.com/site/citronellefluidrockproject).

SUMMARY

Miscible-CO_2 interactions with formation water and reservoir rock can cause short- and long-term changes in formation matrix geochemistry and permeability, thereby affecting the long-term storage capacity and EOR production of the reservoir. Study of the diagenetic history of the Donovan Sand reservoir indicates that carbonate cementation and feldspar dissolution variably occurred during burial and subsequent diagenesis, and served as the main control on primary and secondary porosity development. Early cementation destroyed primary porosity in some intervals, whereas in other places early cement provided the framework for secondary pores developed due to feldspar dissolution produced porosity. We hypothesize that carbonic and sulfuric acid associated with hydrocarbon charging aided in dissolution of feldspar and clay weathering products. The removal of hydrocarbons from grain surfaces during EOR may lead to continued secondary porosity development via acidic or acidified formation waters, thus in essence making the diageneitc history of Donovan sandstone a predictive analog for future rock-fluid interactions. We predict that the heterogeneity of the Donovan Sand developed from polyphase mineral precipitation and dissolution in the reservoir matrix is likely responsible for forming preferential flow paths within high porosity zones of the reservoir. Viscous fingering of CO_2 due to differential flow along theses paths could have resulted in the initial increase and subsequent decline in CO_2-EOR of the Donovan Sandstone.

A working physical model of rock-fluid interactions could not be obtained for this system, likely due to, rock and fluid heterogeneity, fracture-dominated flow system. The 2-D and 1-D TOUGHREACT models produced to date have failed to give realistic breakthrough times for both CO2 and waterflood fluids, and do not result in reasonable predictions for either the chemistry or temporal composition trends for the produced water samples collected in this study. Initial problems with injection of CO2 almost certainly resulted in NE-SW vertical fracturing of the reservoir. This hypothesis is supported by both water chemistry and oil production data. The presence of the fracturing is a major control on the chemical composition of the produced water samples and has presented serious challenges for constructing a reactive transport model for the system.

REFERENCES

Claypool, G., & Mancini, E., 1989, Geochemical relationships of petroleum in Mesozoic reservoirs to carbonate source rocks of Jurassic Smackover Formation, southwestern Alabama. AAPG Bulletin, 1(1), 904–924.

Coffindaffer, K. 2012, Reservoir Heterogeneity in a Carbon Sequestration Target: The Donovan Sand Member of the Rodessa Formation, Citronelle Field, Alabama: Unpublished M.S. Thesis, West Virginia University.

Donahoe, R.J., Donovan, T., and Weislogel, A. (2013) Injection of supercritical CO2 at Citronelle Field, Mobile County, Alabama, for carbon utilization and storage: Fluid-rock interactions and preliminary modeling results. *AAPG Search and Discovery Article #90163*, 2013 AAPG Annual Convention and Exhibition, Pittsburgh, PA, May 19-22, 2013.

Esposito, R. A., Pashin, J. C., & Walsh, P. M., 2008, Citronelle Dome: A giant opportunity for multizone carbon storage and enhanced oil recovery in the Mississippi Interior Salt Basin of Alabama. Environmental Geosciences, 15(2), 53–62. doi:10.1306/eg.07250707012

Esposito, R. A., 2010, Business models for commercial-scale carbon dioxide sequestration ; with focus on storage capacity and enhanced oil recovery in Citronelle Dome: unpublished PhD Dissertation. University of Alabama at Birmingham.

Fedo, C. M., Nesbitt, H. W., and Young, G. M., 1995, Unraveling the effects of potassium metasomatism in sedimentary rocks and paleosols, with implications for paleoweathering conditions and provenance: Geology, v. 23, no. 10, p. 921-924.

Heydari, E., and C.H. Moore, 1989, Burial diagenesis and thermochemical sulfate reduction, Smackover Formation, southeastern Mississippi salt basin: Geology, v. 17, p. 1080-1084.

Kuuskraa, V. A., R. Lynch, and M. Fokin, 2004, Site selection and process identification for CO2 capture and storage test centers, summary report: Geologic assessment of CO2 storage options, four proposed Southern Company power plants. Prepared under Agreement E2-P79/C5887 for the Electric Power Research Institute by Advanced Resources International, Arlington, Virginia, March 26, 2004, 184 p.

Mancini, E. A., and Puckett, M. T., 2002, Transgressive-regressive cycles in Lower Cretaceous strata, Mississippi Interior Salt Basin area of the northeastern Gulf of Mexico, USA. Cretaceous Research, 23(3), 409–438. doi:10.1006/cres.2002.1012

McLennan, S. M., Hemming, S., McDaniel, D. K., and Hanson, G. N., 1993, Geochemical approaches to sedimentation, provenance, and tectonics: Special Paper - Geological Society of America, v. 284, p. 21-40.